Effect of anisotropic yielding on the flow liquefaction of loose sand

S. M. Reza Imam[1], Dave H. Chan[2], Peter K. Robertson[2], and Norbert R. Morgenstern[3]

Corresponding author:
Norbert R. Morgenstern
Department of Civil and Environmental Engineering
University of Alberta, Edmonton, Alberta, Canada, T6G 2G7

submitted to
Soils and Foundations
Paper No. 2582

Submitted: Nov 27, 2000
Revised: September, 2001

---

1 Former post-doctoral fellow, University of Alberta; Faculty member, Shahid Chamran University, Ahvaz, Iran

2 Professor, Department of Civil and Environmental Engineering, University of Alberta

3 University professor, Department of Civil and Environmental Engineering, University of Alberta

EFFECT OF ANISOTROPIC YIELDING ON THE FLOW LIQUEFACTION OF LOOSE SAND

Abstract

In very loose sand, the ratio M_p of shear stress to mean normal stress at the peak point of the undrained effective stress path (UESP) is very close to the stress ratio M at the peak point of the capped yield surface. Stress ratios M_p can therefore be used in constructing yield surfaces of sands. These stress ratios have also been used in the past in evaluating flow potential of loose sand. Application of M_p for these purposes requires that factors affecting this stress ratio, and quantitative relationships for the variation of M_p with these factors be determined. In this paper, effects of the intermediate principal stress and direction of loading on M_p are investigated, and models are developed by which these effects can be quantified. It is shown that variations of M_p with these factors are similar to the variations of yielding stresses obtained from stress-strain data. Yield surfaces obtained from the variation of M_p indicated a strong dependency of yielding stresses on inherent anisotropy. Data examined in this paper also suggest that the effects of inherent anisotropy on yielding stresses are controlled primarily by the relative magnitudes of the normal stresses applied in the principal directions of material anisotropy.

Keywords: Anisotropy, yield surface, loose sand, liquefaction, constitutive modeling, instability

(IGC: D6; E6; E7)

INTRODUCTION

Loose sands experience loss of shear strength when subjected to undrained loading. This loss of strength decreases at higher densities and disappears when density is sufficiently high. In sands that experience loss of shear strength in undrained loading, the undrained effective stress path (UESP) plotted in a plane of shear stress vs mean normal stress exhibits a peak (Figure 1).

Experimental evidence have indicated that the peak point of the UESP (P-UESP) of loose sand is close to the point of peak shear stress on the capped yield surface (P-YS) (see Imam et al., 2002). Therefore, the variation of the stress state at the P-UESP can be used in the construction of yield surfaces of sands. Obtaining yield surfaces from stress-strain data often requires conducting tests with complex stress paths and interpretation of results of such tests involve significant effort. Moreover, since sands exhibiting loss of shear strength in undrained loading are subjected to flow liquefaction, knowledge of states of stress at the P-UESP is also required in studies of the susceptibility of loose sandy soils to flow failure.

Past studies of the state of stress at the P-UESP have often been qualitative. However, quantitative relationships are required if this stress state is to be used in the construction of yield surfaces and prediction of flow failures.

Effects of void ratio and consolidation stresses on the P-UESP were examined previously (see Imam et al. 2002). Effects of direction of loading and intermediate principal stress are investigated in this paper.

PREVIOUS STUDIES

Yamada and Ishihara (1981) conducted undrained true triaxial tests (TTT) in which samples of loose sand were subjected to loading in octahedral plane which varied from a condition corresponding to triaxial compression (TC) to that of triaxial extension (TE). Test results indicated that as loading condition varies from TC to TE, mobilized shear stress at the P-UESP decreases. Results of hollow cylinder (HC) tests by Symes et al. (1984) and Shibuya and Hight (1987) showed that the ratio of "stress difference," q_d, defined as:

$$q_d = (\sigma_1 - \sigma_3) \tag{1}$$

to the mean normal stress $p = (\sigma_1+\sigma_2+\sigma_3)/3$ at the P-UESP decreases with the angle α_σ between the direction of major principal stress σ_1 and the direction of soil deposition. Similar results were obtained by Uthayakumar and Vaid (1998), and Yoshimine et al. (1998), who also showed that as the parameter b defined by Bishop (1971) as:

$$b = \frac{(\sigma_2 - \sigma_3)}{(\sigma_1 - \sigma_3)} \tag{2}$$

increases, the ratio q_d / p at the P-UESP generally decreases.

The effect of anisotropy on the failure strength of sands has been investigated extensively in the past (see e.g. Arthur and Menzies, 1972, Oda, 1972). Researchers have indicated that strength anisotropy of sand is affected by various factors among them are sand density (Yamada and Ishihara, 1979), mode of failure (Lade, 1982) and strain level (Ochiai and Lade, 1983). Test data have shown that mobilized friction angle at failure is affected by the relative magnitudes of principal stresses, and more significantly, by the direction of their application relative to bedding planes (Lam and Tatsuoka, 1988). Effects of anisotropy and intermediate principal stress on the yielding stresses, however, have been addressed less frequently.

Yield surfaces derived from stress-strain behavior of isotropically consolidated (IC) sands often reflect inherent anisotropy in sands. Yamada and Ishihara (1979) used TTT's to obtain yield surfaces. The surfaces resembled circles in octahedral plane which gradually changed to rounded triangles at higher shear stresses. Due to inherent anisotropy, centers of the yield surfaces were shifted such that higher yielding stresses were obtained when loading was applied in the direction of soil deposition. The yield and failure surfaces obtained by Pradel et al. (1990) and Gutierrez et al. (1993) from results of HC tests showed similar indications of inherent anisotropy.

In this paper, variations of the stress state at the P-UESP with the intermediate principal stress and the direction of loading are first examined and correlated separately. Relationships which can account for both effects are then developed. It is shown that the stress state at the P-UESP varies with these factors in the same way as yielding stresses derived from stress-strain data vary, and that both variations reflect inherent anisotropy of sand. Yield surfaces obtained here have also been used in modeling the constitutive behavior of sand and in quantitative assessments of the susceptibility of sand to flow liquefaction (see Imam, 1999).

STATE OF STRESS AT THE P-UESP

The state of stress at P-UESP will be expressed in terms of stress ratio $M_p = q / p$, in which q is the deviatoric stress which can be defined as follows in terms of principal stresses:

$$q = \left[\frac{1}{2}\left((\sigma_1 - \sigma_2)^2 + (\sigma_1 - \sigma_3)^2 + (\sigma_2 - \sigma_3)^2\right)\right]^{1/2} \tag{3}$$

where σ_1, σ_2, and σ_3 are the major, intermediate, and minor effective principal stresses respectively.

UESP's obtained from TC, TE and HC tests are often expressed in terms of q_d (Eq. 1) vs. p; and the effect of σ_2 is expressed in terms of parameter b (Eq. 2). Values of q and q_d are related by the following equation:

$$q = (1-b+b^2)^{1/2}\, q_d \tag{4}$$

and are the same in TC and TE loading in which b is 0 and 1 respectively. Equation 4 also relates the stress ratio:

$$M_{pd} = q_d / p \qquad (5)$$

to stress ratio $M_p = q/p$, both of which defined at the P-UESP.

In anisotropic sand, principal stresses alone cannot fully describe the state of stress since response to loading depends also on the direction of loading relative to the direction of soil anisotropy. The majority of practical applications both in field and in laboratory involve anisotropy in one direction, which is the direction at which soil is deposited (this is assumed to be the z-direction here). In order to investigate the behavior of such cross-isotropic soils, it is sufficient to examine loading with α_σ between 0 and 90 degrees in the zx plane only (see Figure 1). Changes in α_σ in the zy plane will produce the same response, and changes in α_σ in the xy plane will not affect the behavior because the soil is isotropic in this plane.

In general loading of a cross-isotropic soil, b can vary between 0 and 1 and α_σ between 0 and 90 degrees. In TC tests, b = 0 and α_σ = 0 degrees, and in TE tests, b = 1 and α_σ = 90. Therefore, in TC and TE tests, the soil is subjected to combinations of b and α_σ that are in the two opposite extremes.

EFFECTS OF INTERMEDIATE PRINCIPAL STRESS AND DIRECTION OF LOADING ON M_P

Yoshimine (1996) conducted extensive studies on the effects of b and α_σ on the undrained behavior of Toyoura sand using the HC apparatus. Samples at three ranges of void ratio were tested under constant values of b and α_σ. Certain combinations of b and α_σ were selected such that unacceptable non-uniformities would not develop in the HC sample. Therefore, combinations of b and α_σ did not cover the full ranges of possible variations of these parameters. All samples were consolidated isotropically to 100 kPa before shearing.

Variations of $\sin\varphi_p$ with void ratio obtained from the aforementioned HC tests are shown in Figure 2 for various combinations of b and α_σ. Examination of these results indicates that $\sin\varphi_p$ decreases with α_σ and, in most cases, decreases slightly with b. These results are consistent with those of Shibuya and Hight (1987), Uthayakumar (1996) and Yoshimine et al. (1998) who indicated that M_{pd} or φ_p generally decrease with increase in α_σ and/or b. Figure 2 also shows that slopes of lines connecting values of $\sin\varphi_p$ corresponding to the same combination of b and α_σ are close to one another.

Imam et al. (2002) showed that values of $\sin\varphi_p$ obtained from TE tests are smaller than those obtained from TC tests and, in Toyoura sand, slopes of variation of $\sin\varphi_p$ with void ratio obtained from TC and TE tests are similar. These results are consistent with those shown in Figure 2. It may also be noticed from Figure 2 that values of $\sin\varphi_p$ obtained from loading under combinations of b and α_σ which are equivalent to TC and TE approximately constitute, respectively, the upper and lower limits to the variation of $\sin\varphi_p$ with b and α_σ for samples with the same void ratio. The value of $\sin\varphi_p$ for $\alpha_\sigma = 0$ and $b = 0.25$ is slightly larger than that for $\alpha_\sigma = 0$ and $b = 0$ which corresponds to TC loading.

In Figure 3-a, variations of M_{pd} with void ratio of Syncrude sand loaded in TC, TE, and HC with $b = 0.5$ and α_σ between 0 and 90 degrees are shown. Although the HC tests were conducted under a b-value different from those of TC and TE, as α_σ changes from 0 to 90 degrees, M_{pd} varies from a value close to that of TC to a value close to that of TE. The direction of loading, α_σ, therefore, accounts for a major part of the observed difference in M_{pd} between

TC and TE. In Figure 3-b, a similar plot is shown for Toyoura sand tested in HC under b=0 and b=0.5. Although the available HC data did not cover the full range of variation of α_σ, they nevertheless exhibit a behavior similar to that of Syncrude sand.

In order to relate stress states at the P-UESP for various values of b and α_σ, stress functions that can appropriately account for the effects of these factors should be obtained. In the following sections, the effect of b is considered first, and α_σ is examined later.

EFFECT OF THE INTERMEDIATE PRINCIPAL STRESS

Selection of an appropriate stress function

We have so far used $\sin\varphi_p$ or M_p to represent stress states at the P-UESP. In order to account for the effects of intermediate principal stress or b-value on this stress state, we seek a stress function f with the following two properties:

1) The function should vary with void ratio regularly (e. g. with the same slope of variation) regardless of b, such that it can be easily correlated with void ratio.

2) Samples with the same void ratio should have values of f at the P-UESP which are independent of b; however, f can vary with α_σ .

HC test results (Figure 2) and triaxial test results (Imam et al. 2002) indicated that unlike M_{pd}, the function $\sin\varphi_p$ approximately satisfies the first condition but does not satisfy the second.

The data shown in Figure 3 are re-plotted in Figure 4 in terms of $\sin\varphi_p$. In Figure 4-a, the value of $\sin\varphi_p$ obtained from the HC test under b = 0.5 and α_σ = 0 is somewhat larger than $\sin\varphi_p$ obtained from TC (b = 0, α_σ = 0); and, the HC value under b = 0.5 and α_σ = 90 is somewhat larger than that of the TE ($b = 1$, $\alpha_\sigma = 90$). Increase in $\sin\varphi_p$ obtained from tests under $b = 0.5$ can also be noted from Figure 4-b, in which the dotted lines connecting the HC results with the same α_σ but different b have higher slopes compared to the solid lines for TC and TE. Data shown in Figure 2 also indicated higher $\sin\varphi_p$ in tests under $b = 0.25$ or $b = 0.5$ compared to those under $b = 0$ or $b = 1$.

When "failure strength" of sands is expressed in terms of friction angle, larger values are often obtained from tests at b of about 0.25 and 0.50 compared to b of 0 or 1. Data comparing friction angles at failure under $b = 1$ with those under $b = 0$ are, however, contradictory (see e. g. Bishop, 1971; Lade, 1975; Matsuoka and Nakai, 1974). The variation of stress state at the P-UESP with b is, therefore, similar to the variation of strength at failure. Imam et al. (2002) showed that soil dilatancy affects the mobilized strength at the P-UESP in the same way as it affects failure strength. The P-UESP, however, is reached at smaller strain level where non-uniformities and localizations, which can alter measured strengths at failure, are nearly absent.

Because of the similarities mentioned above, the following functions used by Drucker-Prager (D-P), Lade and Duncan (1975) (L-D), and Matsuoka and Nakai (1974) (M-N) as yield-failure surfaces for soils are considered for f:

$$f_{D\text{-}P} = J_2/I_1^2 \qquad (6\text{-a})$$

$$f_{L\text{-}D} = I_1^3/I_3 \qquad (6\text{-b})$$

$$f_{M\text{-}N} = I_1 I_2/I_3 \qquad (6\text{-c})$$

in which I_1, I_2 and I_3 are the first, second and third invariants of stress, and J_2 is the second invariant of deviatoric stress. Geometric representations of the above functions, and also the Mohr-Coulomb criteria given by:

$$f_{M\text{-}C} = \sin\varphi = \frac{\sigma_1 - \sigma_3}{\sigma_1 + \sigma_3} \qquad (6\text{-d})$$

in octahedral plane are shown in Figure 5.

Values of $f_{D\text{-}P}$, $f_{L\text{-}D}$, and $f_{M\text{-}N}$ obtained by substituting the data shown in Figure 3 into Equations 6-a to 6-c are plotted in Figure 6. In Figure 6-a, effect of the difference in the b-value under which the TC test and the HC test with $\alpha_\sigma = 0$ were conducted is evident from the decrease in $f_{D\text{-}P}$ corresponding to the HC test. Since $f_{D\text{-}P}$ is a measure of the radius of the circle representing the D-P yield surface (Figure 5), these data indicate that tests under b = 0.5 result in smaller radius for this circle compared to tests under b = 0. On the other hand, it was shown previously that values of $\sin\varphi_p$ were higher under b = 0.5 compared to b = 0. A suitable stress function should therefore produce strengths at b = 0.5 between those given by the $f_{D\text{-}P}$ and $f_{M\text{-}C}$. Figure 5 indicates that $f_{M\text{-}N}$ and $f_{L\text{-}D}$ provide such values. It may be noticed from Figure 6-b and c that although b-value is not the same in the TC, TE and HC results shown, $f_{M\text{-}N}$ and $f_{L\text{-}D}$ obtained from the HC tests vary almost continuously with α_σ between the TC and TE results. Figure 7, in which the data shown in Figure 3-b are plotted, lead to similar conclusions. These results indicate that $f_{M\text{-}N}$ and $f_{L\text{-}D}$ can better account for the effect of b on the stress state at the P-UESP. Note that these "isotropic" functions were used only to account for b and cannot account for the effect of α_σ on the yielding/failure strength.

Representation in Reference Octahedral Plane (ROP)

To examine the suitability of $f_{M\text{-}N}$ and $f_{L\text{-}D}$ for the full range of variation of b, results of tests conducted under the same α_σ but various b will be plotted in octahedral plane. The vector of shear stress defined by:

$$s_i = \sigma_i - p \qquad i = 1,3 \tag{7}$$

and mobilized at point $P(\sigma_1,\sigma_2,\sigma_3)$ corresponding to the P-UESP (see Figure 8), can be represented in octahedral plane by its magnitude "s" and the angle θ defined by:

$$s = (s_1^2 + s_2^2 + s_3^2)^{1/2} = \sqrt{\frac{2}{3}}\, q \tag{8}$$

$$\theta = \tan^{-1}\left[\frac{\sqrt{3}(\sigma_2 - \sigma_3)}{2\sigma_1 - \sigma_2 - \sigma_3}\right] = 30 + \tan^{-1}\frac{(2b-1)}{\sqrt{3}} \qquad 0 \le \theta \le 60 \tag{9}$$

Stress states P obtained from various tests may not, in general, lie on the same octahedral plane since their corresponding values of p_p may not be the same. A "reference octahedral plane" (ROP) is therefore defined in principal stress space which intersects the hydrostatic axis at point A (1,1,1). Magnitude of the stress ratio vector s_i/p will be represented in this plane as the distance between point A and the intersection of the ROP with the s_i/p line (Figure 8). Values of M_p can therefore be plotted in ROP using the following relationship:

$$M_p = \sqrt{\frac{3}{2}}\,\frac{s_p}{p_p} \tag{10}$$

Values of M_p measured from the HC tests conducted by Yoshimine (1996) are plotted in the ROP in Figure 9. Curves obtained from $f_{M\text{-}N}$ (Equation 6-c) are also shown in the same figure. It may be noticed that:

1. Data points obtained from tests under the same α_σ but different b represent curves similar to those of the M-N criteria, indicating that stress states at P-UESP and at yielding/failure vary similarly with b.
2. For samples tested at the same b and void ratio, M_p generally decreases with α_σ.
3. Curves of constant α_σ are not centered at the center of the ROP; rather, they are translated in the direction of s_1/p.

4. Although the available data points were not sufficient to accommodate a general conclusion, the current results were consistent with a constant translation of the centers of the curves regardless of α_σ.

Use of the L-D yield-failure criteria was equally appropriate and did not alter the above conclusions. Since the samples were not pre-sheared and are therefore not expected to exhibit stress-induced anisotropy, the translations of the curves can be attributed to soil inherent anisotropy.

Changes in soil property with α_σ are often used as indications of inherent anisotropy. It is interesting to note, however, that although each curve in Figure 9 represents loading under constant α_σ, strong anisotropy effects are exhibited by the soil merely due to loading under different θ's (i. e. different values of parameter b). Yamada and Ishihara (1979) determined yield loci by connecting points of equal shear strains from "drained" TTT and obtained similar yield surfaces with translated centers.

Translation of the center of the yield curves due to anisotropy can be represented by a vector a (a_1, a_2, a_3) in the ROP with its magnitude, denoted here by the scalar "a," used as a measure of inherent anisotropy.

It was noted earlier that for each void ratio, the same value of "a" was used in Figure 9 for all curves regardless of α_σ. Toyoura sand data presented by Imam et al. (2000) exhibited a nearly constant difference (a_p) between values of $\sin\varphi_p$ measured in TC and TE regardless of void ratio. Constant values of "a" and "a_p" are indications of a constant degree of sand anisotropy regardless of loading direction and void ratio. The difference between mobilized stresses at the P-UESP in TC and TE may therefore provide a measure of inherent anisotropy in sands.

EFFECT OF DIRECTION OF LOADING

Representation of states of stress

In order to examine the effect of α_σ on the mobilized stress at the P-UESP, results obtained from tests on samples with the same void ratio but various α_σ will be represented by Mohr diagrams in which α_σ appears as an independent variable. Since stress states from different tests do not generally lie on the same Mohr circle, the Mohr diagram will be normalized by dividing its abscissa and ordinate by $\sigma_m=(\sigma_1+\sigma_3)/2$. The radius of the Mohr circle in this diagram can be obtained as follows in terms of principal stresses or stresses obtained from HC tests :

$$R = \frac{\sigma_1 - \sigma_3}{\sigma_1 + \sigma_3} = \sqrt{\left(\frac{\sigma_z - \sigma_x}{\sigma_m}\right)^2 + \left(\frac{\sigma_{zx}}{\sigma_m}\right)^2} = \sin\varphi \tag{11}$$

in which σ_z and σ_x are normal stresses acting in the z and x directions respectively, and σ_{zx} is the shear stress. The resulting diagram will be referred to as the "Reference Mohr Diagram" (RMD), with R being the radius of the "Reference Mohr Circle" (RMC) in this diagram (Figure 10). The coordinates of the center of the RMC in the RMD are (1,0) and the radius equals $\sin\varphi$ regardless of the magnitudes of the principal stresses. Since strengths expressed in terms of friction angles are functions of intermediate principal stress, each RMC will be used for results with the same b. In such diagrams, changes in the radius of the RMC, R_p, with α_σ represent variations of $\sin\varphi_p$ with the direction of loading.

Correlating experimental results

Data shown in Figure 9 are plotted in Figure 11 using the RMD. From this figure, it may be noticed that:

1. The radius $R_p = \sin\varphi_p$, decreases with α_σ
2. Variations of R_p with α_σ can be approximated by circles with their centers shifted in the $\alpha_\sigma = 0$ direction. This shift, which can be attributed to sand inherent anisotropy, is referred to here as a'_p.
3. Although the parameter a'_p may not be constant for each sand in general, constant values of a'_p could be used to model the data for each sand in Figure 11.
4. The radius R_p varies with b. Compared to cases with b=0 or b=1, values of R_p for b of about 0.5 or 0.25 are generally higher. These changes in $\sin\phi_p$ with b are similar to the changes in friction angle at failure of soils with b.

Similar conclusions can be reached from Figure 11-b and c obtained from tests on two other sands. While for Toyoura sand $a'_p = 0.12$, Fraser River sand and Syncude sand exhibited $a'_p = 0.07$ and $a'_p = 0.06$ respectively, reflecting smaller anisotropies.

If the radius of the shifted circle is denoted by R'_p, the value of R_p can be obtained for any α_σ from the following equation which is evident from the geometry of Figure 10:

$$R_p = a'_p \cos 2\alpha_\sigma + [\, R'^{2}_p - (a'_p \sin 2\alpha_\sigma)^2 \,]^{1/2} \qquad (12)$$

The average value of $\sin\varphi_p$ (i.e. R'_p) varies with b and its variation can be obtained from functions such as $f_{L\text{-}D}$ or $f_{M\text{-}N}$ discussed previously.

Pradel et al. (1990) obtained circular yield surfaces in a coordinate system with the abscissa of $X=\dfrac{\sigma_z - \sigma_x}{2\sigma_m}$ and ordinate $Y=\dfrac{\sigma_{zx}}{\sigma_m}$. Centers of these circles were shifted from the origin due to anisotropy. Circular failure surfaces obtained by Gutierrez et al. (1993) using a similar procedure exhibited similar shift due to anisotropy. Tests conducted during these two studies had a b-value of 0.5. Variation of the stress state at P-UESP investigated here is similar to the variation of yielding/failure stresses obtained from stress-strain data in these two studies and further indicate that these results may also apply to other values of b.

THE COMBINED EFFECT OF b AND α_σ

A measure of inherent anisotropy in sands

Different quantities were used to account for sand anisotropy when effects of each of b and α_σ was examined separately before. However, since both of these quantities are related to anisotropy, it is preferable to use a single parameter which can reflect anisotropy as observed in both cases. Using a single parameter, it is easier to determine response to loadings with various combinations of b and α_σ and to interpret results of simple tests with pre-determined combinations of b and α_σ, such as TC (b=0, α_σ=0) and TE (b=1, α_σ=90) tests. Both b and α_σ corresponding to TC are different from those at TE and therefore, TC and TE results cannot be used to isolate effects of b and α_σ.

From the interpretation of experimental results presented below we seek a single measure of sand anisotropy which is related to both b and α_σ.

Experimental observations on the combined effects of b and α_σ

Consider states of stress in the true triaxial tests (TTT) conducted by Yamada and Ishihara (1979) in which p was kept constant while shear stresses were increased along different radii on the octahedral plane (Figure 12). The position of each loading radius can be determined by an angle θ defined in terms of principal stresses σ_x, σ_y and σ_z as:

$$\theta = \tan^{-1}\left[\frac{\sqrt{3}(\sigma_x - \sigma_y)}{2\sigma_z - \sigma_x - \sigma_y}\right] \qquad 0 \le \theta \le 180 \qquad (13)$$

The angle θ is measured clockwise from the ZC-direction such that $\theta = 0$ corresponds to TC loading in z-direction (ie. ZC) and $\theta = 180$ corresponds to ZE. In TTT test, σ_z always remains the principal stress and is the major principal stress when $0 \le \theta \le 60$, the intermediate principal stress when $60 \le \theta \le 120$, and the minor principal stress when $120 \le \theta \le 180$. The magnitude of σ_z compared to σ_y and σ_x decreases with θ. The shear stresses at yielding, plotted in octahedral plane, also decrease with θ as shown in Figure 12.

If α_σ is defined for TTT's in the same way as it was defined previously for the HC tests, it may be noticed from Figure 12 that for $\theta < 60$, σ_z is the major principal stress and therefore $\alpha_\sigma = 0$; but when θ slightly exceeds 60 degrees, α_σ changes to 90 degrees since σ_z is no longer the major principal stress. However, despite this discontinuous change in α_σ, the magnitude of σ_z, and also the yielding stress, changes continuously with θ at $\theta = 60$ (see Figure 12). Note, however, that at $\theta = 60$, the intermediate and major principal stresses are equal. Therefore, the angle α_σ alone may not, in general, provide a suitable measure of change in soil properties due to sand anisotropy.

In HC tests on samples deposited in the z-direction, normal stresses σ_x, σ_y, σ_z may not be the principal stresses. These stresses, and the shear stress σ_{zx}, can be determined for any given values of $0 \le \alpha_\sigma \le 90$ and $0 \le \theta \le 60$ (Equation 9) from the following equations:

$$\sigma_z = p - \frac{s}{\sqrt{6}}\left(\sin(\theta - 30) - \sqrt{3}\cos(\theta - 30)\cos 2\alpha_\sigma\right) \qquad (14\text{-a})$$

$$\sigma_x = p - \frac{s}{\sqrt{6}}\left(\sin(\theta - 30) + \sqrt{3}\cos(\theta - 30)\cos 2\alpha_\sigma\right) \tag{14-b}$$

$$\sigma_y = p + \frac{2s}{\sqrt{6}}\sin(\theta - 30) \tag{14-c}$$

$$\sigma_{zx} = \frac{s}{\sqrt{2}}\cos(\theta - 30)\sin 2\alpha_\sigma \tag{14-d}$$

Equation 14-a indicates that in loadings under constant p and s, σ_z decreases with α_σ and/or θ (or b). Experimental results shown in Figure 9 indicate that M_p also decreases with α_σ and/or b. Therefore, M_p and σ_z are affected similarly by changes in α_σ or b.

The aforementioned examinations of results of TTT and HC tests suggests that changes in M_p due to anisotropy in cross-isotropic sand may be related to the relative magnitude of the normal stress σ_z applied in the direction of anisotropy compared to the normal stresses σ_x and σ_y applied in the other two directions. This was true regardless of whether the normal stresses were principal stresses (as in TTT) or not (as in HC tests).

MODELING THE VARIATION OF M_P IN INHERENTLY ANISOTROPIC SAND

In sand deposited in the z-direction and which exhibits its strongest response in this direction, if the x-y-z directions remain principal directions during shearing (as is usually the case in triaxial tests and TTT's), the variation of M_p in the ROP of the principal stress space $O\sigma_x\sigma_y\sigma_z$ can be represented as shown in Figure 13. In this case, principal axes of anisotropy and principal axes of applied stresses coincide. In Figure 13, if the direction of the shearing vector *s* is defined by a unit vector u_s, and if the direction of anisotropy vector a (a_x, a_y, a_z) is given by a unit vector u_a such that:

$$u_s = \frac{s_p}{\mathrm{s_p}} \tag{15-a}$$

$$u_a = \frac{a}{\mathrm{a}} \tag{15-b}$$

the angle θ between the two directions can be obtained from:

$$\cos\theta = u_s\, u_a \tag{16}$$

Using Equation 16 and the geometry of Figure 13, the stress ratio M_p can be determined form:

$$M_p = a\, u_s\, u_a + [\overline{M}_p^{\,2} - a^2 + (a\, u_s\, u_a)^2\,]^{1/2} \tag{17}$$

in which M_p and $\overline{M}_p$ are magnitudes of vectors M_p and $\overline{M}_p$ respectively and we have:

$$M_p = \mathrm{M_p}\, u_s \tag{18}$$

$$\overline{M}_p = M_p - a \tag{19}$$

The variation of $\overline{M}_p$ in the ROP can be defined by the following isotropic relationship (Gudehus, 1973), which produces shapes similar to those obtained from the Matsuoka-Nakai (1974) and the Lade Duncan (1975) yield-failure criteria. This equation, however, has a simpler algebraic form and provides more flexibility in matching experimental results:

$$\overline{M}_p = \overline{M}_{p,c}\; g(\bar{\theta}) \tag{20}$$

$$g(\bar{\theta}) = \frac{2c}{(1+c) - (1-c)\cos 3\bar{\theta}} \tag{21}$$

$$c = \frac{\overline{M}_{p,e}}{\overline{M}_{p,c}} \tag{22}$$

in which c is a constant. The following relationships, derived from the geometry of Figure 13, and using Equation 22 can be used to obtain "a" and $\overline{M}_{p,c}$:

$$\overline{M}_{p,c} = M_{p,c} - a \tag{23}$$

$$a = \frac{cM_{p,c} - M_{p,e}}{1+c} \tag{24}$$

Stress ratios $M_{p,c}$ and $M_{p,e}$ are obtained directly from triaxial tests or correlations which will be given later. These stress ratios, and consequently stress ratios $\overline{M}_{p,c}$ and $\overline{M}_{p,e}$, are functions of void ratio and mean normal stress (p).

Parameters "c" and "a" can be obtained independently if sufficient experimental data (ie. variations of M_p with b) is available; otherwise, one of them may be approximated and the other obtained from the relationships given before. In constitutive modeling of sand behavior, the c-value was approximated by the ratio of stress ratios (M) at steady state obtained from TE and TC (see Imam, 1999).

It was noticed previously that the variation of $\sin\varphi_p$ is related linearly with void ratio "e." The following equations were obtained by Imam et al. (2002) for cases in which mean normal stresses are not high:

$$\sin\varphi_{p,c} = \sin\varphi_\mu - k_p\,(e - e_\mu) \qquad \text{for TC} \tag{25-a}$$

$$\sin\varphi_{p,e} = \sin\varphi_\mu - a_p - k_p\,(e - e_\mu) \qquad \text{for TE} \tag{25-b}$$

in which $\varphi_{p,c}$ and $\varphi_{p,e}$ are the friction angles at P-UESP in TC and TE tests respectively, e_μ is the void ratio corresponding to φ_μ, k_p is the slope of variation, and a_p is the difference between $\sin\varphi_p$ in TC and TE. The friction angle φ_μ and the void ratio e_μ are coordinates of a reference point on the TC line (Equation 25-a) by which the position of this line is determined. The angle φ_μ can be selected to be close to the inter-particle friction angle. Once $\sin\varphi_p$ is determined from Equation 25, values of $M_{p,c}$ and $M_{p,e}$ are obtained from:

$$\text{(a)}\ M_{p,c} = \frac{6\sin\varphi_p}{(3-\sin\varphi_p)} \qquad \text{(b)}\ M_{p,e} = \frac{6\sin\varphi_p}{(3+\sin\varphi_p)} \tag{26}$$

The angle $\overline{\theta}$ is related to θ (Equation 13) by the following equation obtained from the geometry of Figure 13 and using Equations 20 to 22:

$$(1-c)\ a \sin\theta \cos 3\overline{\theta} + 2\ c\ \overline{M}_{p,c} \sin(\overline{\theta}-\theta) - (1+c)a \sin\theta = 0 \tag{27}$$

In HC tests, principal directions of anisotropy and applied stresses are not the same. However, experimental results shown in Figure 9 indicate that the variation of M_p in the ROP of the principal stress space $O\sigma_1\sigma_2\sigma_3$ constitute rounded triangles similar to that from which Equation 17 was derived. The sizes of these triangles were a function of α_σ.

Stress conditions in HC tests are often expressed in terms of the four components of stress tensor given by Equation 14. It is shown here that in this case M_p can be approximated by Equation 17 provided that the unit vectors u_s and u_a in the principal stress space are replaced by their equivalent unit tensors in the general stress space, and the inner product $u_s u_a$ is replaced by double contraction of the two unit tensors. The unit tensor u_s will have four non-zero components in HC tests; and u_a will have its principal directions oriented in the principal direction of material anisotropy and will have three non-zero components in the x-y-z directions.

Equations 14 and 15-a can be used to obtain the following components of u_s for HC tests by considering that $s_{ij} = \sigma_{ij} - p\ \delta_{ij}$ (δ_{ij} is the Kronecker delta):

$$u_{s,zz} = \frac{1}{\sqrt{6}} [\sqrt{3} \cos(\theta\text{-}30) \cos 2\alpha_\sigma - \sin(\theta\text{-}30)] \tag{28-a}$$

$$u_{s,xx} = \frac{1}{\sqrt{6}} [-\sqrt{3} \cos(\theta\text{-}30) \cos 2\alpha_\sigma - \sin(\theta\text{-}30)] \tag{28-b}$$

$$u_{s,yy} = \frac{2}{\sqrt{6}} \sin(\theta\text{ -}30) \tag{28-c}$$

$$u_{s,zx} = \frac{1}{\sqrt{6}} \cos(\theta\text{-}30) \sin 2\alpha_\sigma \tag{28-d}$$

Components of u_a can be obtained from Equations 28 by substituting $\theta = 0$ and $\alpha_\sigma = 0$. Note that the shear stress component of u_s will not affect $u_s u_a$ since its corresponding component in u_a is zero. This result is consistent with the previously discussed interpretation of TTT and HC test results that the effect of anisotropy on the yielding stresses is controlled primarily by the normal stresses applied in the principal directions of material anisotropy.

In TTT, principal directions of applied stresses and anisotropy coincide and components of u_s can be determined by substituting for $\alpha_\sigma = 0$ in Equations 28. When sand is deposited in the z-direction, these equations can also be used to obtain components of u_a by substituting for $\theta =$ 0.

The relationships obtained previously were used to model the HC results shown in Figure 9. A constant c=0.85 obtained from the stress ratios at steady state was used for all the correlations. Variations of $M_{p,c}$ and $M_{p,e}$ with void ratio were obtained by substituting for $k_p =$ 1.5, $e_\mu = 0.88$, $\varphi_\mu = 23$ and $a_p = 0.25$ in Equations 25. These values were approximated from the HC results shown in Figure 2. However, only TC and TE test results are, in general, sufficient to obtain these parameters if HC and triaxial test results are consistent. Modeled and measured values of M_p are shown in Figure 14 and are generally in good agreement. It may be noticed that although the HC tests were conducted under values of α_σ which varied at equal increments of 15 degrees, consecutive contours of M_p obtained from these tests are not equidistant from each other; and the proposed model replicates such behavior correctly.

SUMMARY AND CONCLUSIONS

Effects of intermediate principal stress (or b) and direction of loading (α_σ) on stress ratio M_p at the peak point of the undrained effective stress path (P-UESP) of loose sand were investigated using results of Hollow Cylinder (HC) and Triaxial (TXL) tests. Variations of M_p with b and α_σ were correlated with void ratio and relationships were developed by which these variations can be quantified. It was shown that variations of M_p with b and α_σ are similar to the variations of yielding stresses of sands derived from stress-strain data. Examination of TXL test data have also showed that M_p can be used in the construction of yield surfaces (see Imam et al. 2002).

Effects of inherent anisotropy on the yielding of sand were investigated and modeled using the variation of M_p. These results suggested that in cross-isotropic sand, effect of inherent anisotropy on yielding stresses is primarily controlled by the relative magnitude of the normal stress acting in the principal direction of material anisotropy compared to the normal stresses acting in the other directions. An analytical model for the variation of M_p with intermediate principal stress and direction of loading was developed and provided good estimates of measured values of this stress ratio.

Yield surfaces derived from the variations of M_p obtained herein have been used in modeling the constitutive behavior of sand. Extensive tests with complex stress paths are normally needed in constructing yield surfaces using stress-strain data. Relationships for the variation of

M_p are also needed in quantitative assessments of the susceptibility of loose sandy soils to flow liquefaction (see Imam 1999).

ACKNOWLEDGEMENT

This study was supported in part by the Natural Sciences and Engineering Research Council of Canada, NSERC. The first author would also like to acknowledge the support of the MCHE of Iran during his PhD studies. The help of Dr. M. Yoshimine and Dr. R. Verdugo in providing the first author with digital data of test results on Toyoura sand is also appreciated.

NOTATION:

$\boldsymbol{a}$, a, a_1, a_2, a_3 = Anisotropy vector, representing the translation of the center of yield surface in the "reference octahedral plane," its magnitude and three components

a_p = Difference between $\sin\varphi_p$ of sand with $e = e_\mu$, in triaxial compression and extension

a'_p = Difference between $\sin\varphi_p$ of sand loaded at constant "b" but α_σ of 0 and 90 degrees

b = Parameter representing relative magnitude of intermediate principal stress to major and minor principal stresses

c = Ratio of magnitudes of $\overline{M}_p$ obtained from TC and TE tests

e, e_i = Current and initial (preparation) void ratios

e_μ = Initial void ratio corresponding to mobilized friction angle φ_μ at peak of undrained effective stress path

$f_{D\text{-}P}$ = Drucker-Prager yield-failure stress function, and its numerical value

$f_{L\text{-}D}$ = Lade-Duncan yield-failure stress function, and its numerical value

$f_{M\text{-}N}$ = Matsuoka-Nakai yield-failure stress function, and its numerical value

$f_{M\text{-}C}$ = Mohr-Coulomb yield-failure stress function, and its numerical value

$g(\bar{\theta})$ = Function describing the variation of $\overline{\mathrm{M}}_\mathrm{p}$ with $\bar{\theta}$

k_p = Slope of variation of $\sin\varphi_p$ with void ratio

$\boldsymbol{M_p}$, $\mathrm{M_p}$ = Vector representing the ratio of shear stress to mean normal stress at peak of undrained effective stress path in reference octahedral plane, and its magnitude

$\overline{\boldsymbol{M}}_p$, $\overline{\mathrm{M}}_\mathrm{p}$ = The isotropic component of $\boldsymbol{M_p}$ and its magnitude

$\overline{\mathrm{M}}_{\mathrm{p,c}}$, $\overline{\mathrm{M}}_{\mathrm{p,e}}$ = Magnitudes of $\overline{\boldsymbol{M}}_p$ in TC and TE

$\mathrm{M_{p,c}}$, $\mathrm{M_{p,e}}$ = Stress ratios $\mathrm{M_p}$ in triaxial compression and triaxial extension

$\mathrm{M_{pd}}$ = Ratio of stress difference to mean normal stress at peak of undrained effective stress path

$\mathrm{M_{p,c}}$, $\mathrm{M_{p,e}}$ = Stress ratios $\mathrm{M_p}$ in triaxial compression and triaxial extension

$\mathrm{M_\mu}$ = Stress ratio q/p corresponding to inter-particle friction

$p = (\sigma_1+\sigma_2+\sigma_3)/3$ Effective mean normal stress

p_c, p_p = Effective mean normal stress at consolidation, and at the P-UESP

q_d = Stress difference: difference between major and minor principal stresses

q = Deviatoric stress

R, R_p = Radius of "Reference Mohr Circle" and its value at the P-UESP

s, s, s_1, s_2, s_3 = Vector of applied shear stress in octahedral plane, its magnitude and components in principal stress space

$\mathit{s_p}$, s_p = Shear stress vector at the peak of undrained effective stress path and its magnitude

$\mathit{u_s}$, $\mathit{u_a}$ = Unit vectors in the direction of applied shear stress, and anisotropy

$u_{s,xx}$, $u_{s,yy}$, $u_{s,zz}$, $u_{s,zx}$ = Components of unit vector in the direction of applied shear stress

α_σ = Angle between the direction of major principal stress σ_1 and direction of soil deposition

φ_p = Friction angles at peak of undrained effective stress path

φ_μ = Inter-particle friction angles

θ = Angle between TC direction and loading direction measured in octahedral plane

$\bar{\theta}$ = Angle between TC direction and vector $\overline{M}_p$, measured in octahedral plane

σ_m = Average of major and minor principal stresses

σ_x, σ_y, σ_z = Normal stresses acting in the x, y, and z directions

σ_{zx} = Shear stress acting in direction x in the plane normal to the z axis

REFERENCES

Arthur, J. R. F. and Menzies, B. K., 1972. Inherent Anisotropy in a sand. Geotechnique, **22** (1):115-128.

Been, K. and Jefferies, M. G. 1985. A state parameter for sands. Geotechnique, **35**(2): 99-112.

Bishop, A. W. 1971. Shear strength parameters for undisturbed and remoulded soil specimens. Roscoe Memorial Symposium: 3-58.

Cambou, B. and Lanier, J. 1988. Induced anisotropy in cohesionless soil: Experiments and modelling. Comput Geotech, **6**(4): 291-311.

Chillarige, AnnajiRao, V, Robertson, P. K., Morgenstern, N. R., and Christian, H. A. 1997. Evaluation of the in situ state of Fraser River sand. Canadian Geotechnical Journal, **34**(4): 510-519.

Drucker, D. C. and Prager, W. 1952. Soil Mechanics and Plastic Analysis or Limit Design. Quarterly of Applied Mechanics, **10**: 157-165.

Gudehus, G. 1973. Elastoplastische stoffgleichungen fur trockenen sand. Ingenieur-Archiv, **42**: 151-169.

Gutierrez, M., Ishihara, K., and Towhata, I. 1993. Model for the Deformation of Sand During Rotation of Principal Stress Direction. Soils and Foundation, **33**(3): 105-117.

Hyodo, M., Tanimizu, H., Yasufuku, N., and Murata, H. 1994. Undrained cyclic and monotonic triaxial behavior of saturated loose sand. Soils and Foundations, **34**(1): 19-32.

Imam, S. M. R. 1999. Modeling the constitutive behavior of sand for the analysis of static liquefaction. Ph D thesis, The University of Alberta.

Imam, S. M. R., Morgenstern, N. R., Robertson, P. K. and Chan, D. H. 2002. Yielding and Flow Liquefaction of Loose Sand. Accepted for publication in Soils and Foundations.

Ishihara, K. 1993. Liquefaction and flow failure during earthquakes. Geotechnique, **43**(3): 351-415.

Konrad, J.-M. and Pouliot, N. 1997. Ultimate state of reconstituted and intact samples of deltaic sand. Canadian Geotechnical Journal, **34**(5): 737-748.

Lade, P. V., 1982. Localization Effects in Triaxial Tests on Sand. Proceedings of International Union of Theoretical and Applied Mechanics, Conference on Deformation and Failure of Granular Materials, Delft: 461-471.

Lade, P. V. and Duncan, J. M. 1975. Elasto-plastic stress-strain theory for cohesionless soil. J.of Geotech.Engrg.ASCE GT10: 1037-1051.

Lam, W. K., and Tatsuoka, F. 1988. Effects of Initial Anisotropic Fabric and σ_2 on Strength and Deformation Characteristics of Sand. Soils and Foundations, **28**(1): 89-106.

Matsuoka, H., Nakai, T. 1974. Stress-deformation and strength characteristic of soil under three-different principal stresses, Proc. JSCE, **242**, 59-70.

Oda, M., 1972. Initial Fabrics and Their Relations to Mechanical Properties of Granular Material. Soils and Foundations, **12**(1): 17-36.

Ochiai, H. and Lade, P. V. 1983. Three-dimensional Behavior of Sand with Anisotropic Fabric, Journal of Geotechnical Engineering Division, ASCE, **109**: 1313-1328.

Pradel, D., Ishihara, K., and Gutierrez, M. 1990. Yielding and Flow of Sand Under Principal Stress Axes Rotation. Soils and Foundations, **30**(1): 87-99.

Riemer, M. F. 1992. The Effects of Testing Conditions on the Constitutive Behavior of Loose, Saturated Sands Under Monotonic Loading. PhD Thesis, University of California at Berkeley.

Shibuya, S. and Hight, D. W. 1987. Bounding surface for granular materials. Soils and Foundations, **27**(4): 123-136.

Symes, M. J., Gens, A., and Hight, D. W. 1984. Undrained anisotropy and principal stress rotation in saturated sand. Geotechnique, **34**(1): 11-27.

Thomas, J. 1992. Static, Cyclic and Post-Liquefaction Undrained Behavior of Fraser River Sand. MSc.Thesis, University of British Columbia.

Uthayakumar, M. and Vaid, Y. P. 1998. Static liquefaction of sands under multiaxial loading. Canadian Geotechnical Journal, **35**(2): 273-283.

Vaid, Y. P., Sivathayalan, S., Eliadorani, A., and Uthayakumar, M. 1996. Laboratory testing at UBC. CANLEX report dated April 1996.

Verdugo, R. L. 1992. Characterization of sandy soil behavior under large deformation. Ph D thesis, University of Tokyo.

Wride, C. and Robertson, P. K. 1997. CANLEX Phase I and III, data review report.

Wride, C. and Robertson, P. K. 1997. CANLEX Phase II, Data Review Repot.

Yamada, Y. and Ishihara, K. 1979. Anisotropic deformation characteristics of sand under three dimensional stress conditions. Soils and Foundations, **19**: 79-94.

Yamada, Y. and Ishihara, K. 1981. Undrained deformation characteristics of loose sand under three-dimensional stress conditions. Soils and Foundations, **21**(1): 97-107.

Yasufuku, N., Murata, H., and Hyodo, M. 1991. Yield characteristics of anisotropically consolidated sand under low and high stresses. Soils and Foundations, **31**(1): 95-109.

Yoshimine, M. 1996. Undrained flow deformation of saturated sand under monotonic loading conditions. Ph D thesis, University of Tokyo.

Yoshimine, M., Ishihara, K., and Vargas, W. 1998. Effect of principal stress direction and intermediate principal stress on undrained shear behavior of sand. Soils and Foundations, **38**(3): 179-188.

(1) Sand type	(2) Source	(3) Mineralogy	(4) Angularity	(5)D_{50} (mm)	(6) e_{max}	(7) e_{min}	(8) M_{ss}
Toyoura	Ishihara (1993)	75 % quartz ; 25 % Feldespar	subangular	0.17	0.977	0.597	1.24
Syncrude	Wride & Robertson (1997a)	95% quartz	angular to subangular	0.15	0.958	0.668	1.19
Fraser River	Wride & Robertson (1997b)	(*) 40 % quartz; 11% feldespar; 45% rock fragments etc.	(*) subangular to subrounded	0.3	1.056	0.677	(*) 1.4

(*) Chillarige et al. (1997)

Table 1 Properties of the sands investigated.

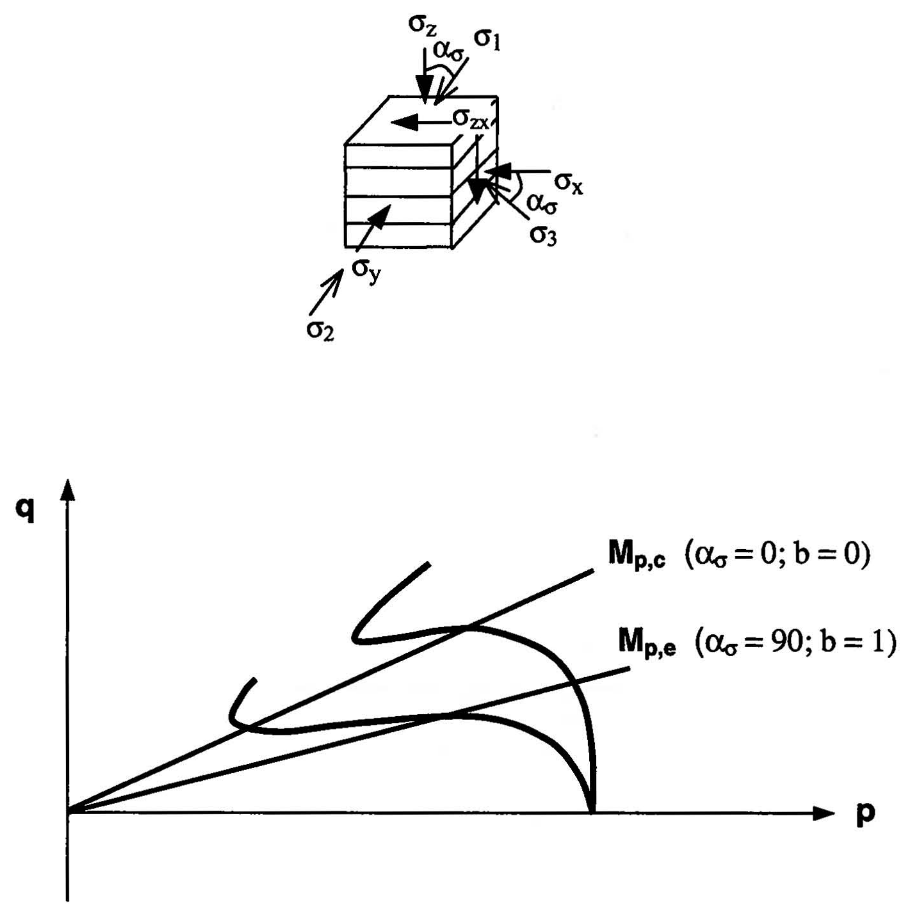

Figure 1 Schematic representation of undrained effective stress paths and stress conditions of loose sand in triaxial compression and extension loading

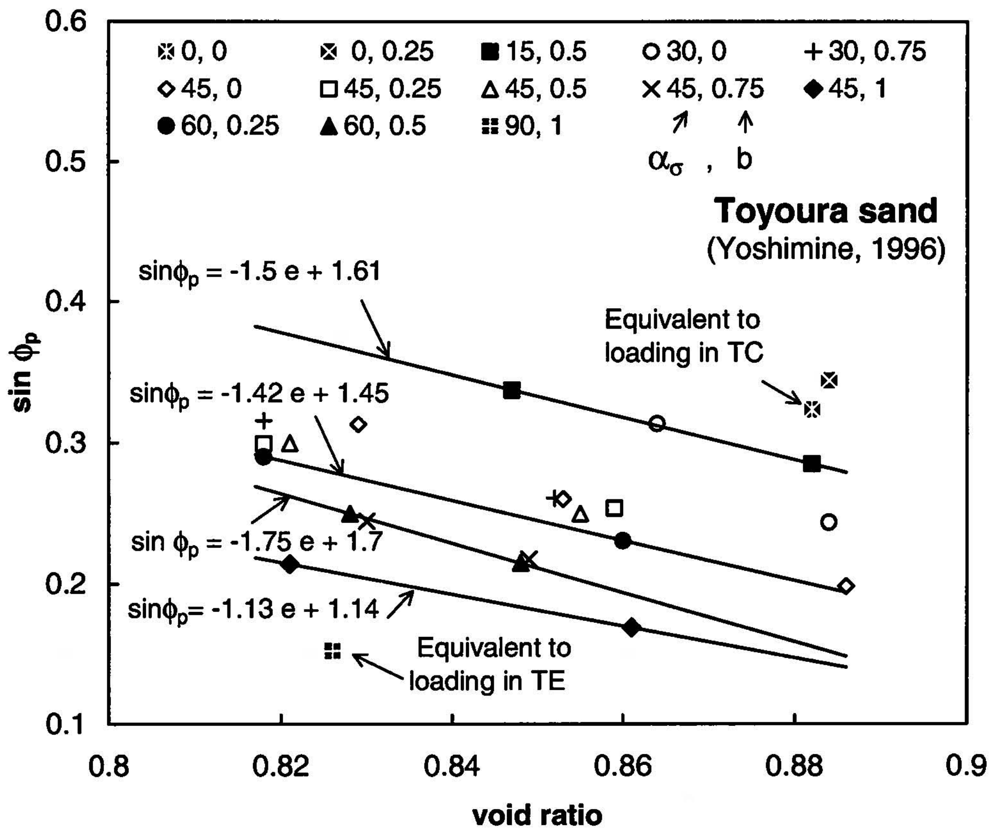

Figure 2 Variation of $\sin\phi_p$ with void ratio for different combinations of b and α_σ as obtained from Hollow Cylinder tests

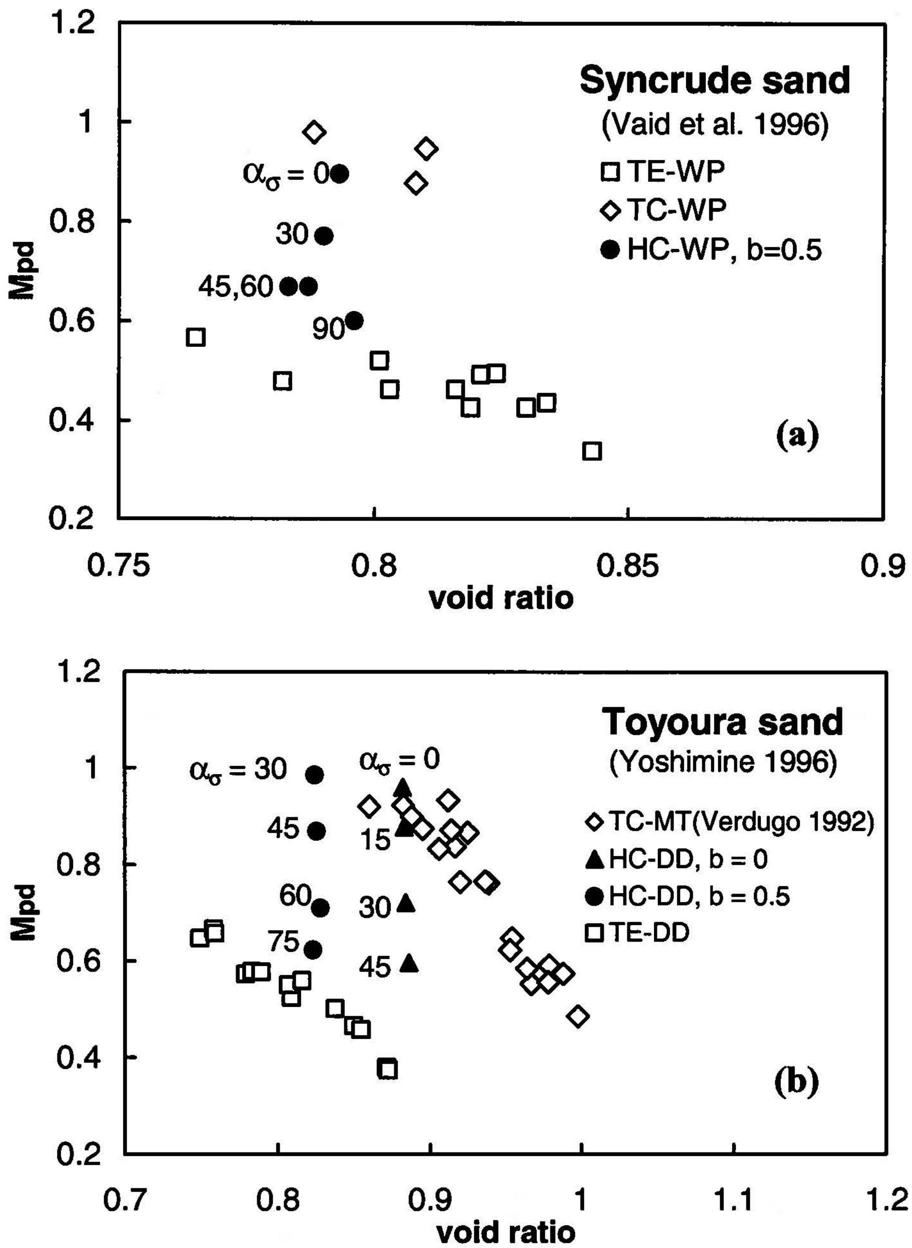

Figure 3 Effect of direction of loading α_σ on M_{1p} in Syncrude sand and Toyoura sand

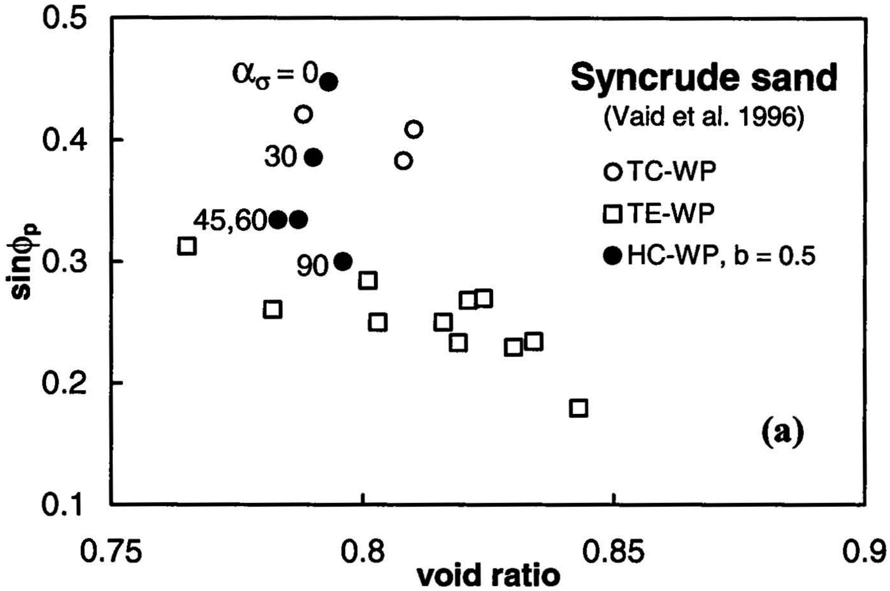

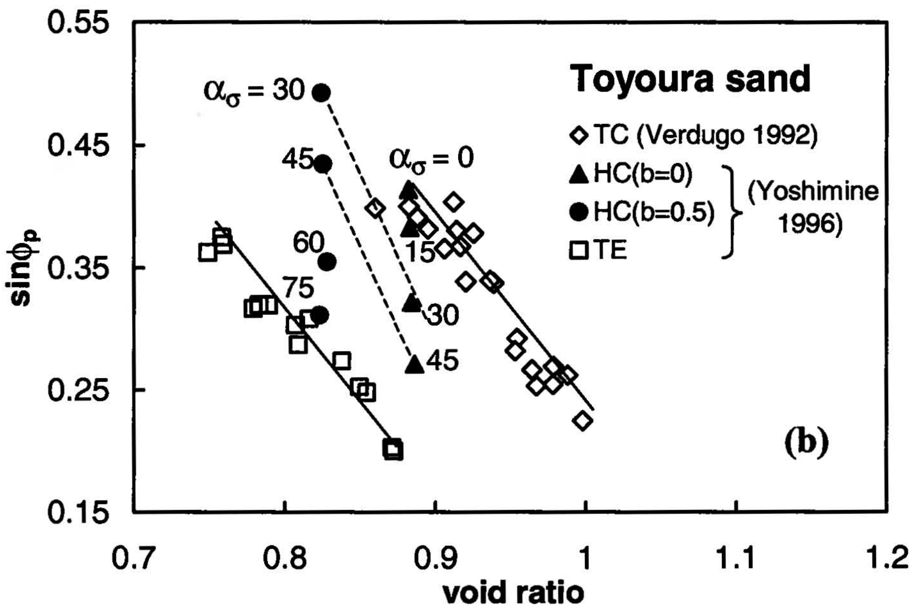

Figure 4 Effects of direction of loading (α_σ) and intermediate principal stress on $\sin\varphi_p$ in Syncrude sand and Toyoura sand

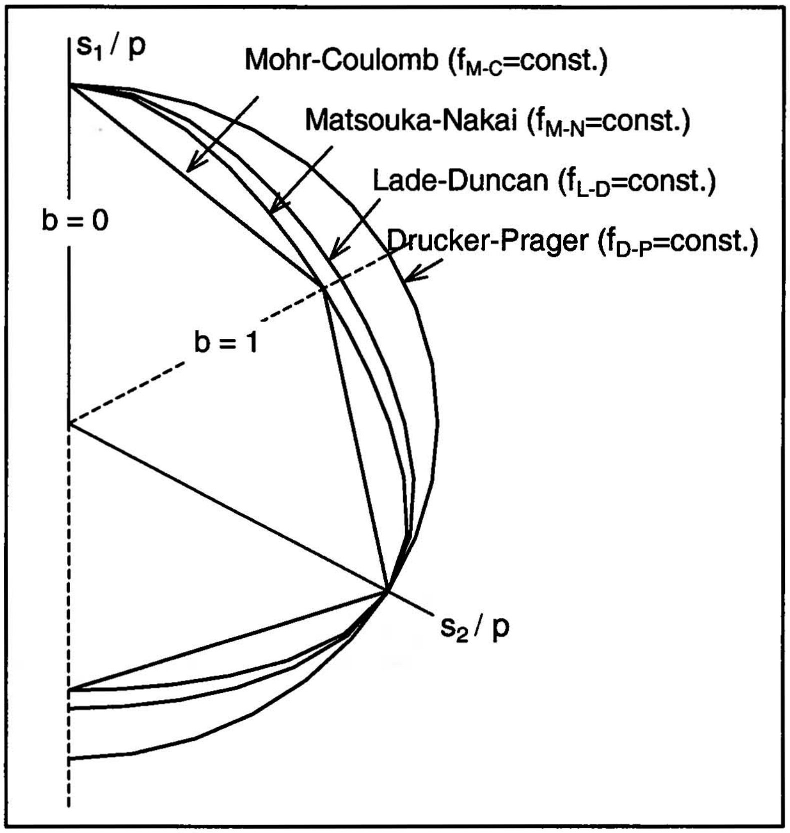

Figure 5 Representation of different yield-failure criteria in octahedral plane

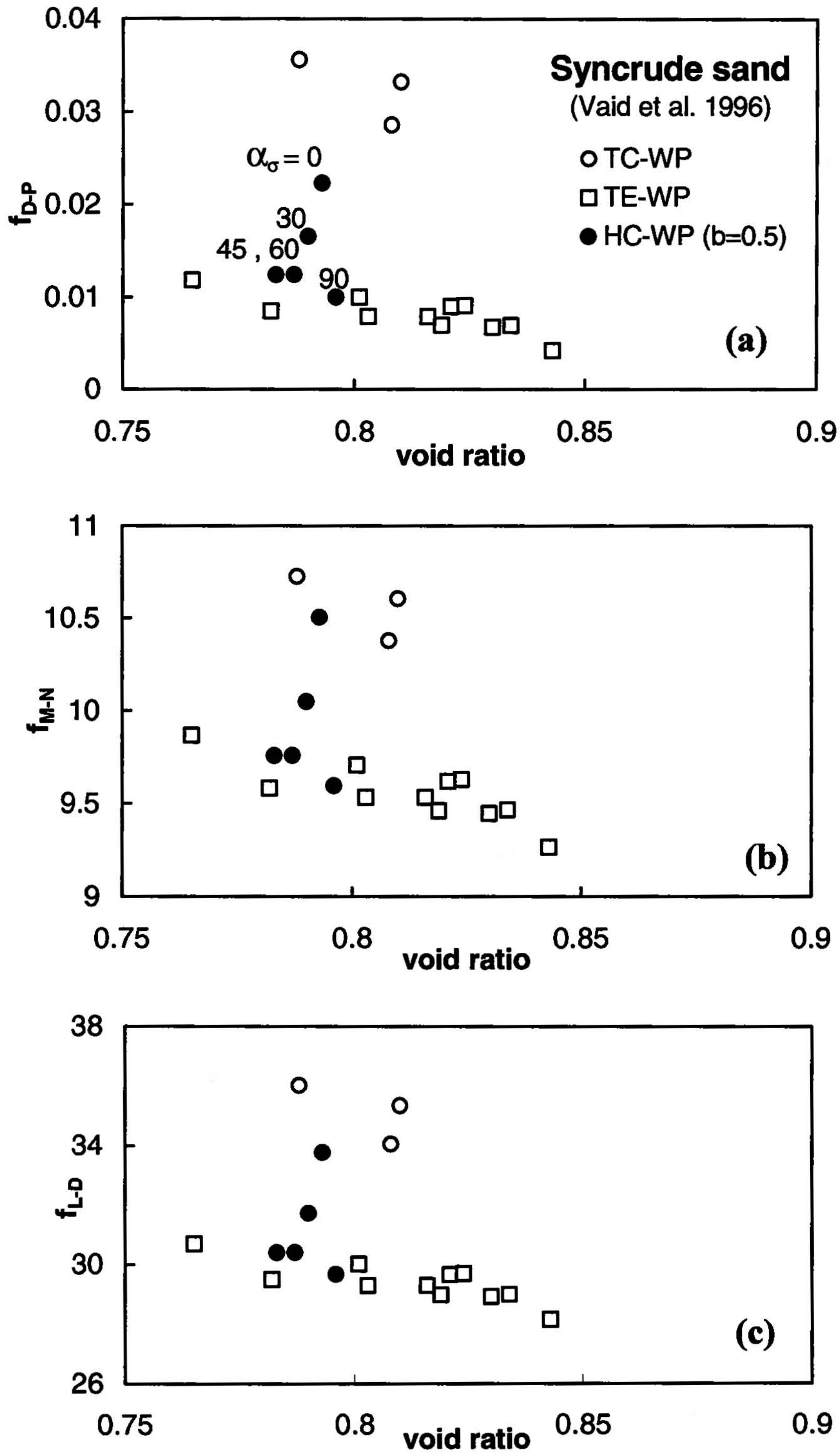

Figure 6 Correlating stress states at P-UESP with void ratio in Syncrude sand, using different yield-failure criteria

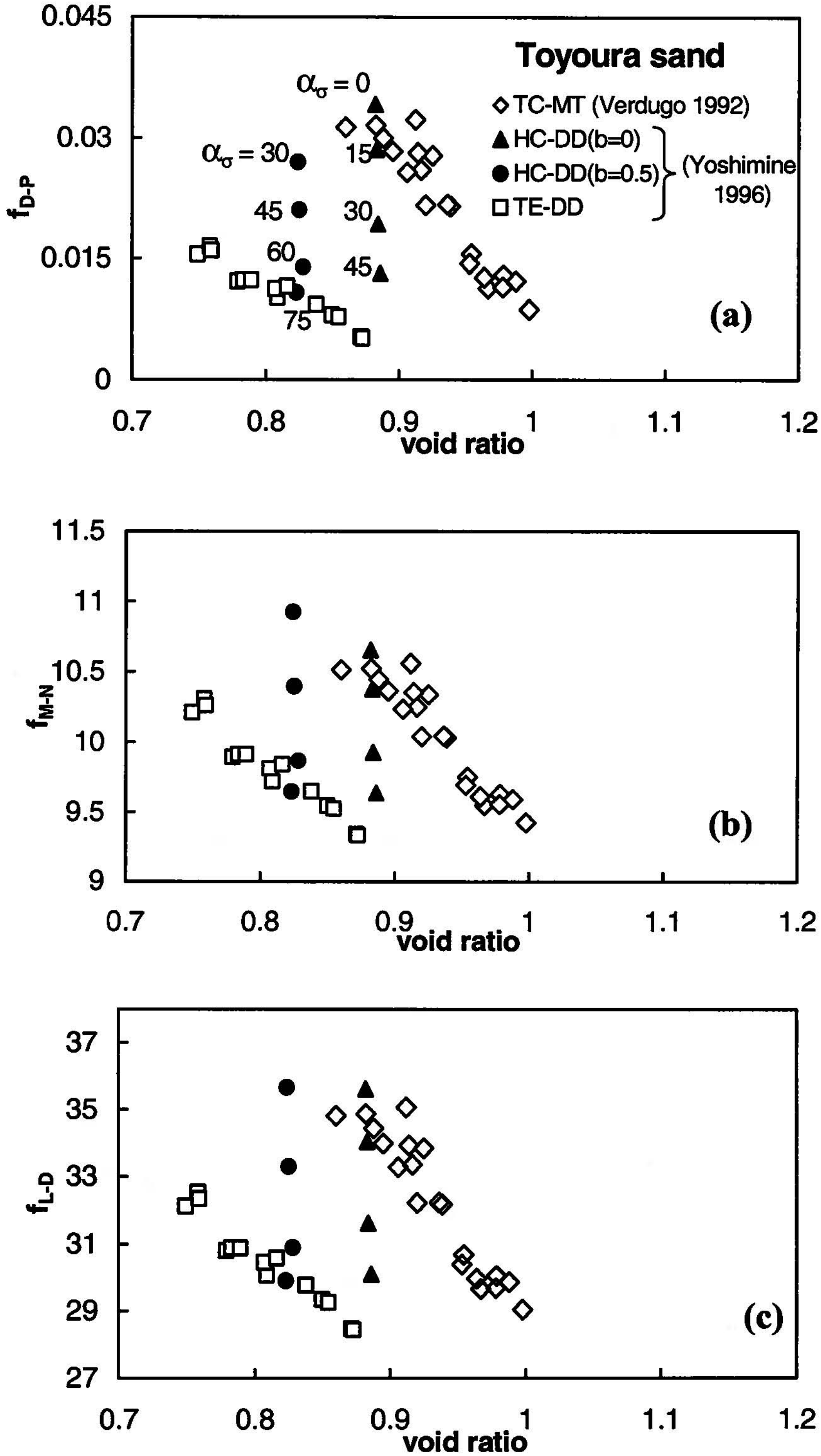

Figure 7 Correlating stress states at P-UESP with void ratio in Toyoura sand, using different yield-failure criteria

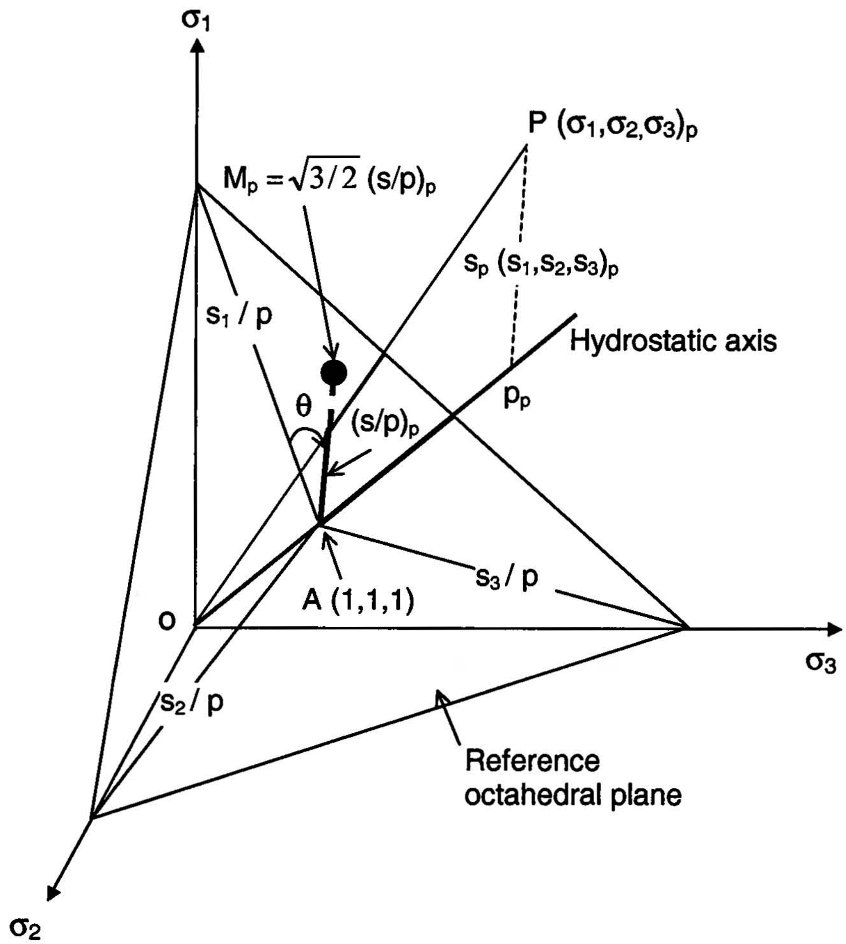

Figure 8 Representation of stress states at the P-UESP in the "Reference Octahedral Plane" (ROP) defined in principal stress space

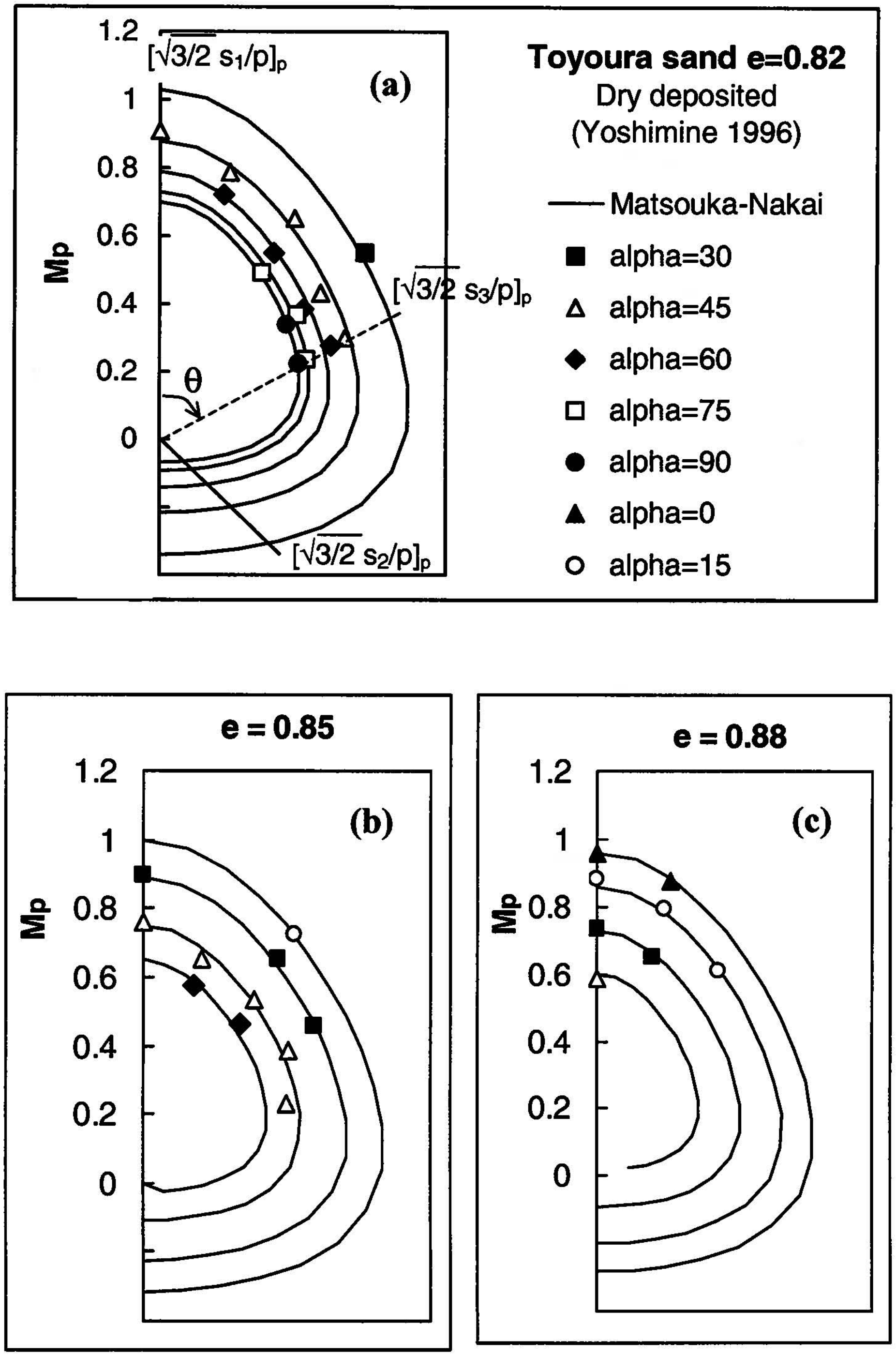

Figure 9 Variation of M_p in Reference Octahedral Plane (ROP) for Toyoura sand

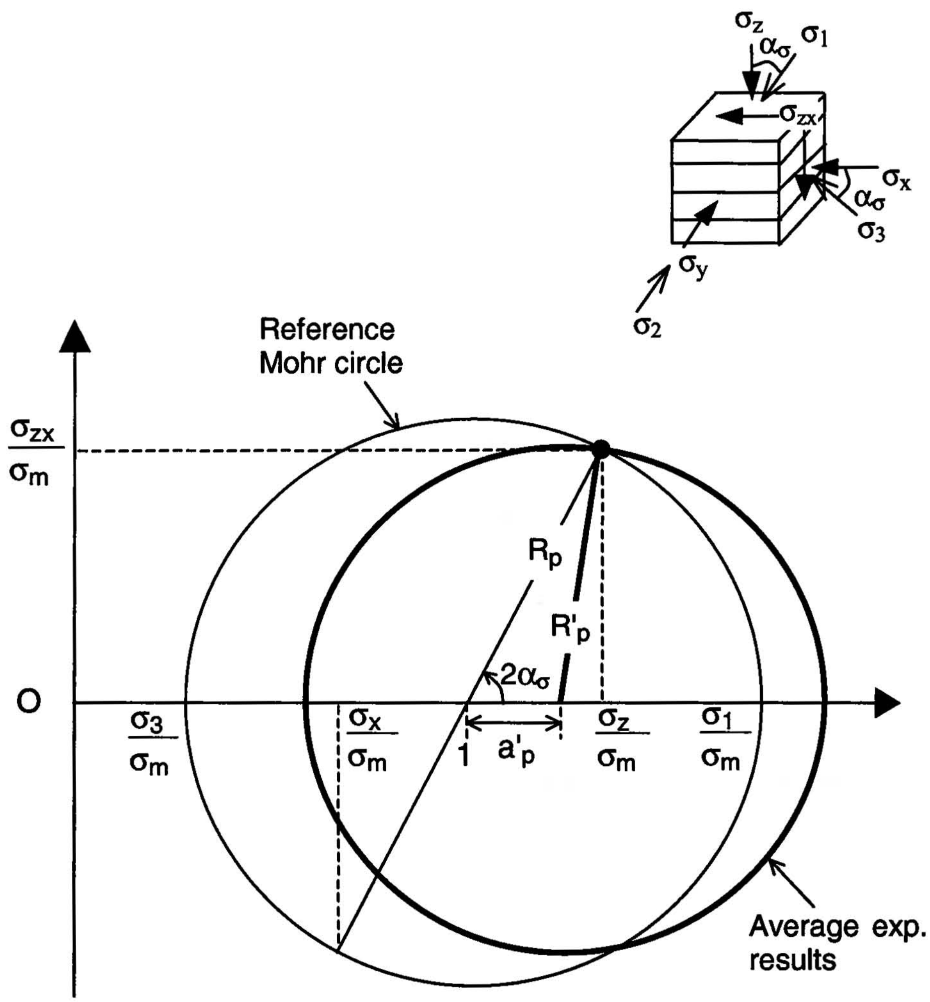

Figure 10 Representation of stress states at P-UESP with the direction of loading α_σ using the reference Mohr Circle (RMC).

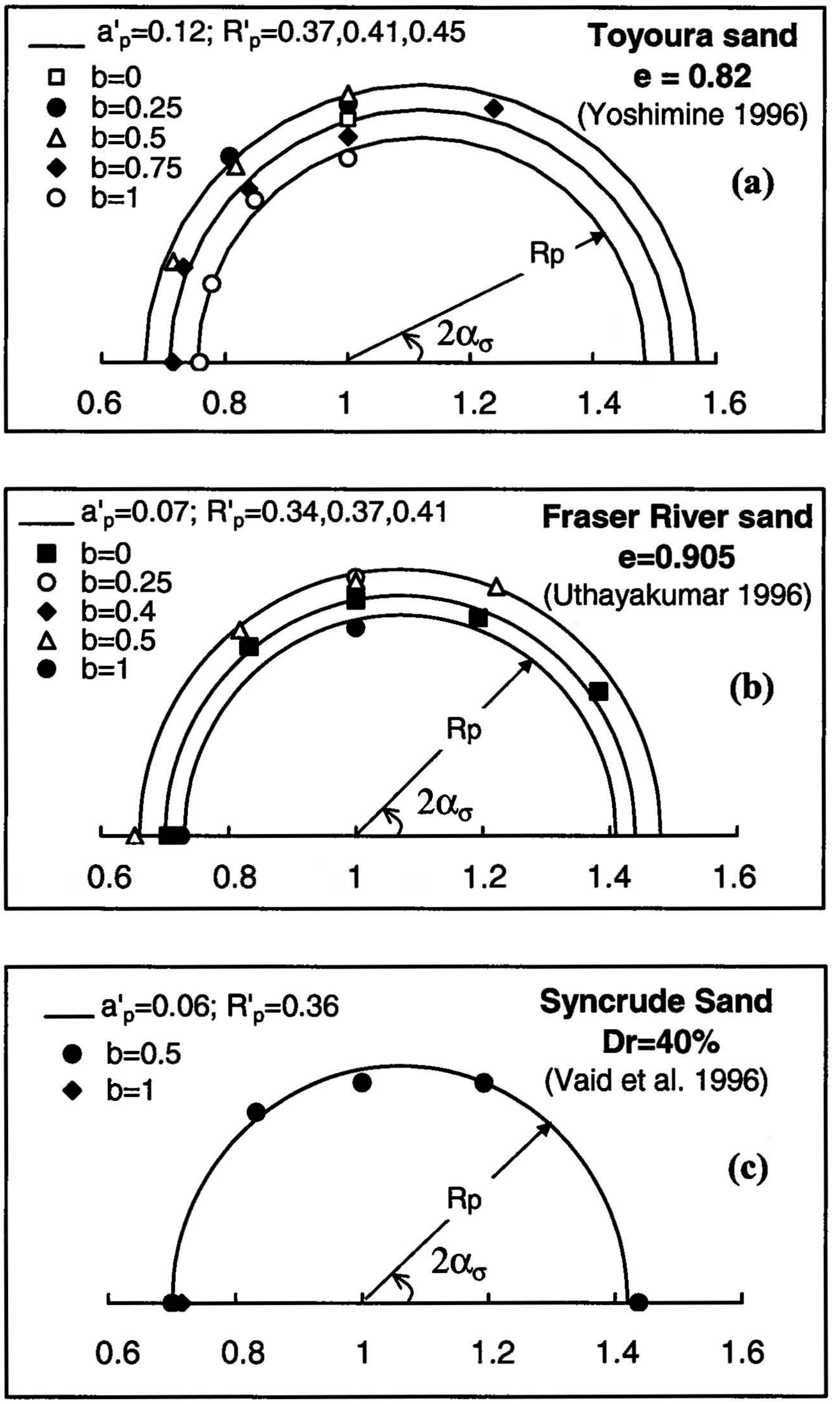

Figure 11 Variations of $R_p=\sin\varphi_p$ with α_σ for different sands as represented in Reference Mohr Diagram

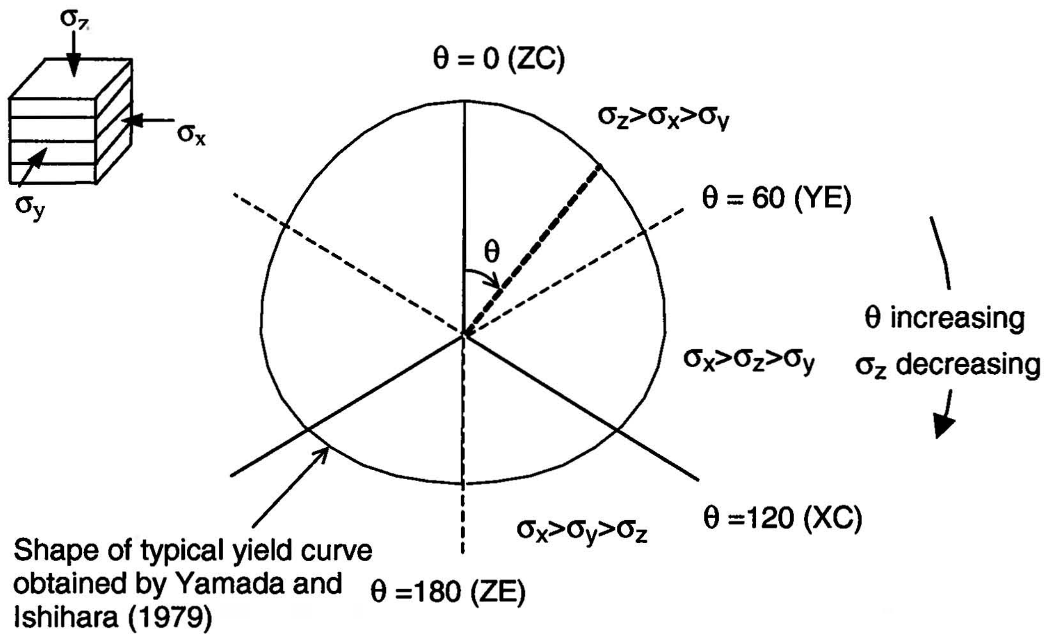

Figure 12 Changes in relative magnitudes of principal stresses with θ in true triaxial test (TTT).

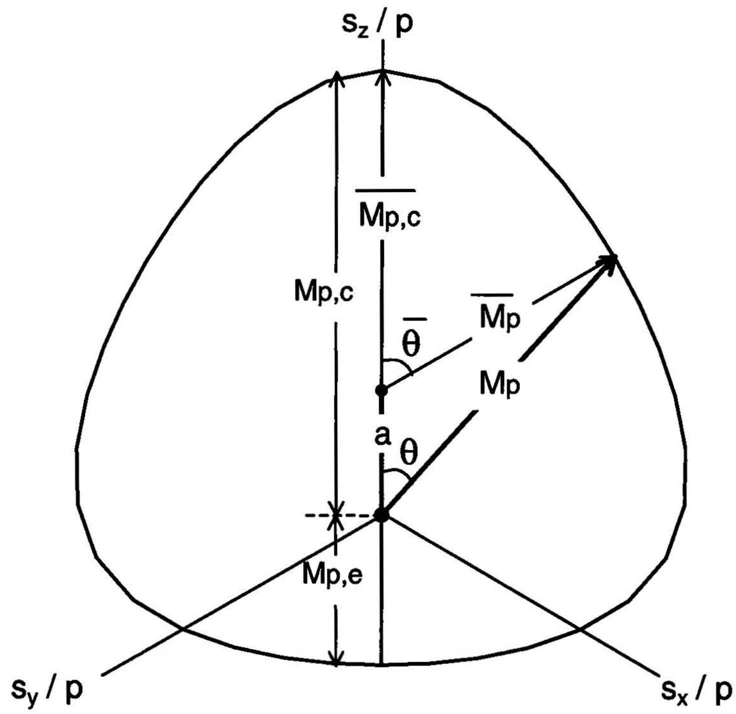

Figure 13 Definition of parameters used in modeling the variation of M_p with b and α_σ

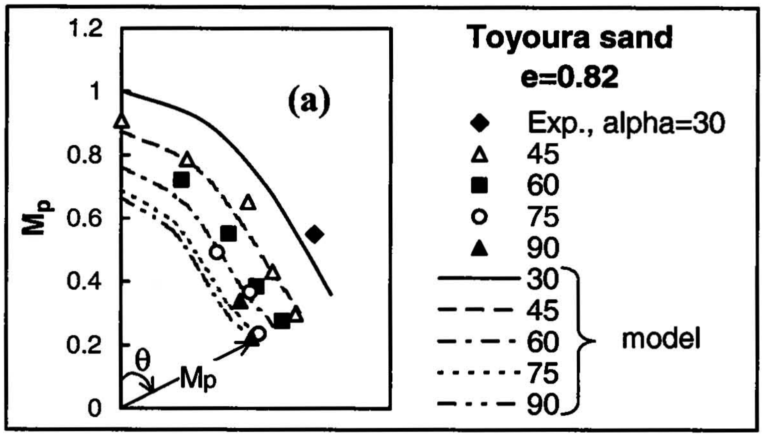

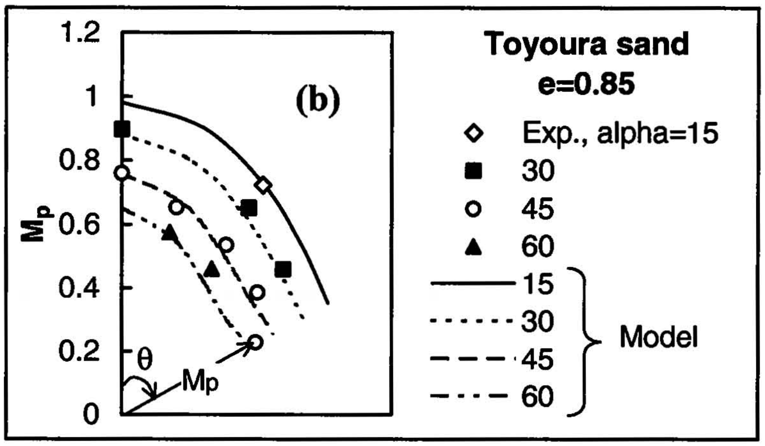

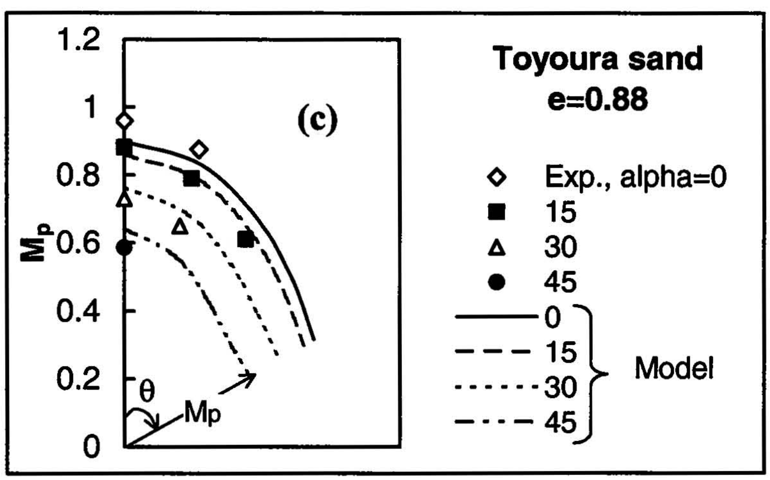

Figure 14 Comparison of modeled and measured variations of M_p with b and α_σ